

Fast Efficient Object Detection Using Selective Attention

Shivanthan Yohanandan^{1,3}, Andy Song¹, Adrian G. Dyer¹,
Angela Faragasso², Subhrajit Roy³, and Dacheng Tao⁴

¹ RMIT University, Melbourne, Australia

{shivanthan.yohanandan, andy.song, adrian.dyer}@rmit.edu.au

² The University of Tokyo, Japan

faragasso@robot.t.u-tokyo.ac.jp

³ IBM Research, Melbourne, Australia

{yohanshi, subhrajit.roy}@aul.ibm.com

⁴ UBTECH Sydney AI Centre, SIT, FEIT, The University of Sydney, Australia

dacheng.tao@sydney.edu.au

Abstract

Deep learning object detectors achieve state-of-the-art accuracy at the expense of high computational overheads, impeding their utilization on embedded systems such as drones. A primary source of these overheads is the exhaustive classification of typically $10^4 - 10^5$ regions per image. Given that most of these regions contain uninformative background, the detector designs seem extremely superfluous and inefficient. In contrast, biological vision systems leverage selective attention for fast and efficient object detection. Recent neuroscientific findings shedding new light on the mechanism behind selective attention allowed us to formulate a new hypothesis of object detection efficiency and subsequently introduce a new object detection paradigm. To that end, we leverage this knowledge to design a novel region proposal network and empirically show that it achieves high object detection performance on the COCO dataset. Moreover, the model uses two to three orders of magnitude fewer computations than state-of-the-art models and consequently achieves inference speeds exceeding 500 frames/s, thereby making it possible to achieve object detection on embedded systems.

1. Introduction

Object detection is a core computer vision task and there is a growing demand for enabling this capability on embedded devices [1]. State-of-the-art deep learning models, such as Faster R-CNN [2], YOLO [3], and SSD [4], achieve unprecedented object detection accuracy at the expense of high computational costs [5]. A major contributor to these

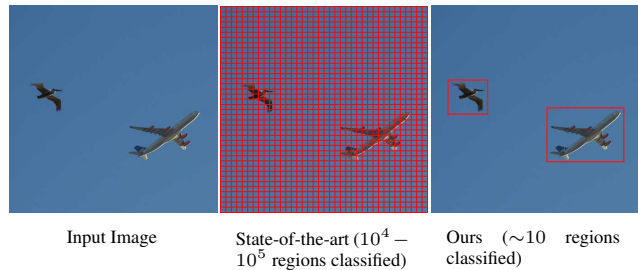


Figure 1: Region proposal filtration comparison. This figure panel compares the number of regions (red boxes) typically classified as containing background or objects by state-of-the-art object detection models with our method. Our method rarely evaluates background regions, thus significantly reduces computational costs.

costs is the exhaustive region proposal generation stage of object detection [6], where typically thousands of regions from an input image are classified as background or object regions prior to sending only object regions for further classification (Figure 1). Since images typically contain more background than objects of interest, most regions evaluated during the region proposal stage contain uninformative background and are therefore processed unnecessarily [7, 8]. To mitigate this computational cost, researchers employed optimization to reduce the network architecture size of these state-of-the-art models (*e.g.* Tiny SSD [9] and SqueezeDet [10]). Nevertheless, these smaller models inherit the same region proposal generation algorithm and consequently still evaluate mostly background regions.

In contrast, object detection in biological vision sys-

tems is extremely efficient owing to the mechanisms behind saliency detection and selective attention [11]. Saliency detection involves the generation of a saliency map in the brain, which spatially maps the locations of salient regions, most likely objects of interest, in the visual field [12]. The brain then selectively attends to these regions serially to process them further *e.g.* classifying objects. Inspired by this mechanism’s speed and efficiency, many attempts have leveraged saliency-based models to generate object-only region proposals in object detection [13, 14, 15, 16, 17]. Unfortunately, none have improved the speed or efficiency over state-of-the-art models.

Intuitively, saliency-based approaches should be able to improve detection efficiency if implemented correctly. Therefore, the pursuit of a deeper understanding of the mechanisms behind saliency detection prompted a thorough investigation of the visual neuroscience literature. Consequently, we discovered that saliency detection is efficient because the retina compresses visual information from the entire visual field by $\sim 90\%$ to a low-resolution achromatic image [18]. This image is then processed by a structure called the superior colliculus (SC), which was only recently identified as the correct location where the saliency map is generated in primates and humans [19, 20, 21]. Such an arrangement has the effect of significantly reducing the visual search space of objects and regions of interest [22], so that a relatively small and simple neural network suffices for computing and generating a saliency map. In contrast, most saliency-guided object detection models typically employed high-resolution (*e.g.* 800×600 pixels [14]) color images to train and run their detection models, which could explain their high computation costs. However, a recent study [11] investigated the preservation of saliency in low-resolution grayscale (LG) images and found that saliency was well-preserved in images downsampled all the way to 64×64 pixels.

Inspired by our assumption that LG input into the SC of primates and humans is the primary reason behind speed and efficiency in natural saliency detection, together with the encouraging results from [11], we designed a novel saliency-guided selective attention region proposal network (RPN) and investigated its speed and computational costs. This study provides two main contributions: (1) unveiling the mechanism behind speed and efficiency in selective visual attention; and (2) establishing a new RPN based on this mechanism and demonstrating the significant cost reduction and dramatic speedup over state-of-the-art object detectors.

2. Related work

The sliding-window approach was the leading detection paradigm in classic object detection. However, with the resurgence of deep learning [23], two-stage detectors quickly came to dominate object detection. As pioneered

in the Selective Search work [24], the first stage generates a sparse set of ideally object-only candidate proposals while filtering out the majority of negative locations [25], while the second stage classifies the proposals into object-category classes. Region Proposal Networks (RPN) integrated proposal generation with the second-stage classifier into a single convolution network, forming the Faster R-CNN framework [2], of which numerous extensions have been proposed, *e.g.* [8, 26, 27, 28, 29]. Nevertheless, while two-stage detectors achieved unprecedented accuracies, they were slow. The need to improve speed ushered in the development of one-stage detectors, such as SSD [4] and YOLO [3, 30].

Both one-stage and two-stage object detection methods typically evaluate $10^4 - 10^5$ candidate regions per image; densely covering many different spatial positions, scales, and aspect ratios. In the current state-of-the-art one-stage detector, RetinaNet [7], evaluation (*i.e.* predicting the probability of object presence) of each of these regions is carried by a classification subnet, which is a fully-convolutional neural network comprising five convolutional layers, each with typically 256 filters and each followed by ReLU activations. Input images into these networks are typically rescaled to 800×1366 pixels, from which $10^4 - 10^5$ candidate regions are individually evaluated. Therefore, significant computational costs are incurred. Consequently, the improved speed of one-stage detectors comes at a significant computational cost, which makes them impractical for embedded systems. Moreover, due to the extreme background-to-object class-imbalance in typical images, the exhaustive region classification design seems extremely superfluous and inefficient.

Inspired by the promise of better region proposal efficiency in natural vision, researchers used saliency-based models to generate object-only region proposals for object detection [13, 14, 15, 16, 17]. Their main motivation was that a saliency map, generated non-exhaustively, could highlight regions containing objects, which can then be proposed to an object-category classifier, thereby ignoring background regions altogether and potentially saving thousands of unnecessary classifications. Nevertheless, a primary shortcoming of these previous attempts is that most models used high-resolution color (*e.g.* 1000×600 pixels; RGB [16]) images, which results in the overall detection model still being more computationally expensive and resource demanding than state-of-the-art one- and two-stage detectors. Furthermore, other studies (*e.g.* [31]) used saliency models trained on human eye fixations. A problem with this approach is that not all objects of interest are detected; just objects that grab human attention, which is inadequate for general object detection.

These saliency-based approaches were inspired by the right idea; however, their implementations may not have

been an accurate reflection of how saliency works in natural vision. Consequently, we decided to revisit the concept of a saliency-guided region proposal network, armed with deeper insights into its biological mechanisms. Our research into salience detection and selective attention in natural vision suggests that the processing of low-resolution achromatic visual information from the retina is key to its speed and efficiency. The implementation of these features in our model enable the processing of a significantly reduced image of the original and only regions highlighted in a saliency map, which would simultaneously address the exhaustive region evaluation paradigm of one- and two-stage detectors, and the high-resolution saliency computation paradigm of previous saliency-guided attempts.

3. Selective attention in natural vision

Selective visual attention describes the tendency of visual processing to be confined largely to stimuli that are relevant, *i.e.* salient, while ignoring irrelevant stimuli such as background. It is among the most fundamental of cognitive functions, particularly in humans and other primates for whom vision is the dominant sense [32]. Visual attention relies on a saliency map, which is a well-known precursor for salience detection [21, 33, 34]. This mapping projects the locations of salient and interesting regions in visual space, thus making vision more efficient by narrowing down the regions an observer must attend to in a typically large visual field. Nevertheless, all of this is existing knowledge; therefore, why have we been unable to achieve similar efficiency in computer vision salience detection?

3.1. The superior colliculus

For a long time, research suggested that the saliency map was generated in the primary visual cortex (V1), which is a cortical structure occupying a relatively large portion of the neocortex. However, two recent papers by independent research teams [19, 21] converged on the claim that the saliency map is actually generated in a significantly smaller and more primitive structure called the superior colliculus (SC). Nevertheless, while these studies finally identified the correct brain structure where saliency is computed, they did not reveal what information from the eye is used to generate a saliency map. Identifying the number, structure, and distribution of retinal ganglion cells (RGCs) ¹ projecting to the SC may reveal key insights into the underlying cause of efficiency in human and primate vision systems. Hence, we conducted further research to determine whether any studies specifically investigated the neural circuitry entering the SC from the eye via the retinocollicular (retina to superior colliculus) pathway, since we suspected that a relatively small proportion of information from the eye is used for comput-

¹Final output neurons of the retina

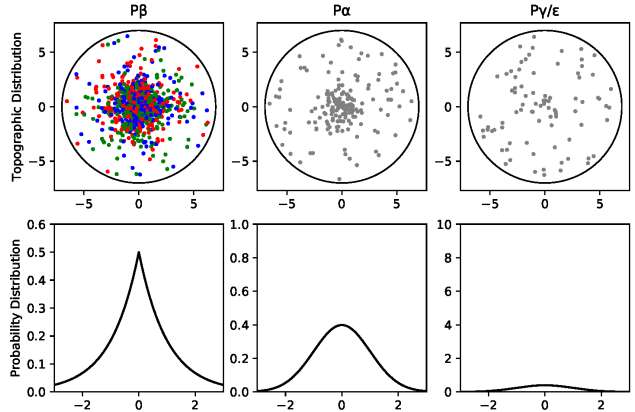


Figure 2: Estimated spatial and cell-type distributions of retinal ganglion cells (RGCs) exiting each eye. $P\beta$ RGCs express color opponency via longwave (red), medium-wave (green), and shortwave (blue) sensitive detectors, and resemble a Laplacian probability density function (PDF). $P\alpha$ and $P\gamma/\epsilon$ are achromatic RGCs encoding primarily luminance information, and resemble Gaussian and Poisson PDFs, respectively. The information and data used to produce these plots were retrieved from [18, 35].

ing saliency, based on a recent study hypothesizing that peripheral vision information was low-resolution and used for computing saliency [11].

3.2. Retinocollicular pathway

Fortunately, two studies by Perry and Cowey in 1984 [18, 35] investigated the neural circuitry entering the SC from the eye via the retinocollicular pathway in the Macaque monkey, which has historically been a good representative animal model for studying primate and human vision. They found that $\sim 80\%$ of all RGCs are $P\beta$ neurons (having small dendritic fields and exhibiting color opponency), projecting axons primarily from the foveal region ² of the retina to the parvocellular lateral geniculate nucleus (LGN) ³. About 10% of RGCs are $P\alpha$ neurons (having large dendritic fields and achromatic output), projecting axons from throughout the retina to magnocellular layers in the LGN. This totals to $\sim 90\%$ of all RGCs projecting to the LGN. The remaining $\sim 10\%$ comprises mainly achromatic $P\gamma$, $P\epsilon$, and (some) $P\alpha$ neurons that are relatively uniformly distributed throughout the retina and only project to the SC. Figure 2 summarizes these estimated RGC distributions.

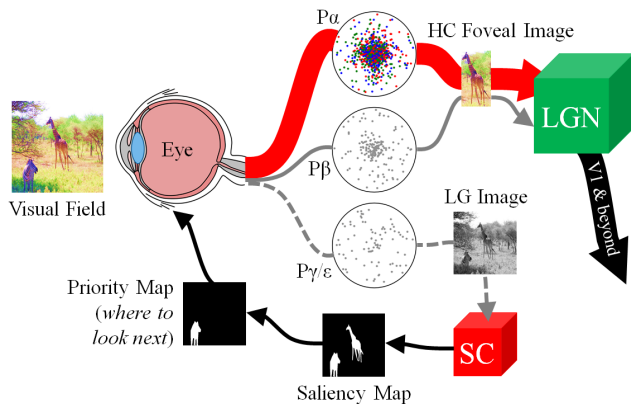


Figure 3: Hypothetical model of selective attention in human and primate vision. An image is first projected onto the retina. The retina then segregates information from this image into different visual pathways. A large chromatic proportion is sent to the LGN and beyond. A significantly smaller achromatic portion is sent to the superior colliculus, where the saliency map is generated.

3.3. A new model of selective attention

En masse, the studies by Perry and Cowey [18,35], Veale [19], and White [21] summarize object detection in human and primate vision as follows: the retinocollicular pathway (dashed gray line in Figure 3) shrinks the high-resolution color image projected onto the retina from the visual field into a tiny colorless, *e.g.* low-resolution grayscale, image, which can then be scanned quickly by the SC to highlight peripheral regions worth attending to via the saliency map. The SC then aligns the fovea to attend to one of these regions, thereby sending higher-acuity, *e.g.* high-resolution color, visual information to the LGN and beyond for further processing. In doing so, a new image of the visual field is now projected onto the retina, and the cycle repeats. From this description of the workings of selective attention, we arrived at the model depicted in Figure 3.

3.4. Low-resolution grayscale

The low-resolution grayscale (LG) compression of visual space performed by the retinocollicular pathway has multiple benefits. Firstly, it reduces the visual search space by representing a large detailed visual field using a relatively small population of neurons. This results in enormous efficiency, since it is reasonable to assume that more neurons would be required to represent the high-resolution details of a larger visual search space, resulting in higher computation and thus, energy demands. Secondly, an object

²Central region of highest visual acuity

³An intermediary structure *en route* to the visual cortex where higher cognitive processes analyze the visual information

can be simply defined as something that occupies a region of visual space and is distinguishable from its surroundings. Therefore, high-resolution details about objects, such as texture, patterns, and shape, seem irrelevant and superfluous. Remember, we are first interested in detecting the presence of an object; what its color or other feature-specific properties are seem only essential for classification. Therefore, LG transformation benefits natural vision by requiring a much smaller (*i.e.* efficient) structure (SC) for computing saliency.

Thence, we begin to realize that, at least in human and primate vision, regions of interest are non-exhaustively selected from a spatially compressed grayscale image, unlike the common computer vision practice of exhaustively evaluating thousands of background regions from high-resolution color images. To the authors knowledge, this is the first paper proposing a plausible hypothesis explaining *how* salience detection and selective attention in human and primate vision is fast and efficient. In the next section, a new model is thereby proposed with the aim of verifying the above hypothesis computationally and replicating the benefits of selective attention in computer vision.

4. Computational selective attention model

Our goal is to reduce computational costs associated with exhaustive region classification in object detection; hence, we are only interested in implementing and investigating the portion of the pipeline that generates the saliency map (*i.e.* the dashed gray line and SC in Figure 3).

4.1. Retinocollicular compression

As explained in Section 3.2, $\sim 10\%$ of RGCs carry sparse achromatic information from the full visual field to the SC. This can be approximated as a low-resolution grayscale image in the digital domain. Following methods outlined in [11], we did this compression by first transforming the color space of high-resolution color (HC) images I_{HC} to 8-bit grayscale I_{HG} . We then down-sampled the original image resolution using bicubic interpolation. In their paper, the authors chose 64 pixels as the target low-resolution height since [36] found this to be the resolution with the best resolution-saliency compromise compared to the other resolutions they investigated. However, this may not necessarily be the optimal resolution for our model. Alternatively, we could follow the 10% rule based on Perry and Cowey's study [18] and downsample the original image to 10% of its original size. However, this 10% compression ratio seems specific to Macaque monkeys based on how their retinocollicular pathway evolved in their natural habitats, which might not necessarily be the optimal compression ratio for object detection in computer vision.

Evolutionarily, we can assume that visual regions and stimuli of interest moulded the retinocollicular pathway

in a given species. Therefore, computationally, we can think of objects and regions of interest in the visual environment as being our positive (salient) class, and everything else as background, which is analogous to a training dataset containing images with background and positively labelled object regions. Moreover, since semantically different object detection datasets might have different properties, such as sky datasets containing simple backgrounds vs. street datasets containing complex scenes, we cannot expect a universal one-size-fits-all downsampling size. Therefore, it seems reasonable to hypothesize that the optimal retinocollicular compression resolution depends on the dataset. Hence, different input resolutions are studied in our experiments presented in Section 5.

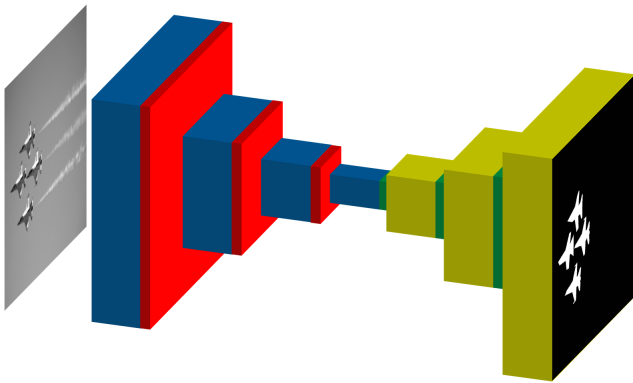


Figure 4: Superior colliculus region proposal network (SC-RPN) architecture. The network takes an input image, adopts convolution layers (blue) with 323×3 kernels and unity stride, together with 2×2 kernel max-pooling layers (red), to transform the image into multidimensional feature representations, before applying a stack of deconvolution layers (yellow) for upsampling the extracted coarse features. Finally, a fully convolution layer with a 1×1 kernel and sigmoid activation function outputs a pixel-wise probability (saliency) map the same size as the input, where larger values correspond to higher saliency.

4.2. Superior colliculus region proposal network

The proposed superior colliculus region proposal network (SC-RPN, Figure 4) simulates partial functionality of the superior colliculus by treating *all* objects and regions of interest or relevance as salient, and subsequently generating a spatial map locating them. Since saliency can be thought of as a single class, the SC essentially behaves as a binary classifier [11]. Therefore, for the purpose of training a binary classifier, we can treat all positive classes (Figure 5B) as the same class (Figure 5C) so that the classifier can generalize saliency across different object classes. This is similar to saliency detection models trained on hu-

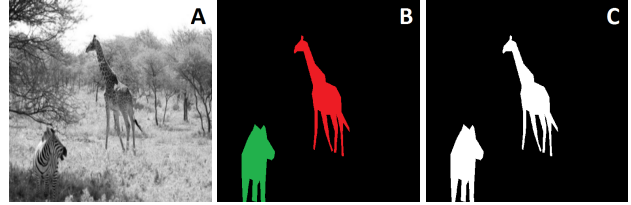


Figure 5: Dataset label binarization. (A) represents the original dataset image, (B) represents the original dataset label where each object class is encoded using a separate pixel value, and (C) is the binarization of B where all object classes are treated as the same positive class and encoded by the same pixel value.

man eye-tracking datasets where fixated objects in an image are assigned the same groundtruth class label despite coming from semantically different object categories. For tasks requiring spatial labels, like generating a pixel-wise mapping of objects, we consider fully convolutional neural networks (FCNs) with deconvolutional layers [37]. This architecture has been previously used for saliency detection in low-resolution grayscale images with great success [11], which is why we used a slightly modified version in our study. The model generates a binary object mapping from a given input, which can then be compared with corresponding groundtruth labels.

5. Experiments

Experiments were conducted to determine (1) whether the SC-RPN could mimic the hypothesized functionality of the biological SC by generating a saliency map that encodes different object categories as the same class; (2) if the optimal retinocollicular compression resolution, *i.e.* smallest input resolution the SC-RPN could detect objects from without significant accuracy loss, is dataset dependent; (3) what impact the optimal resolution has on reducing computation costs and inference times; and (4) how these costs and speeds compared with state-of-the-art RPNs (*i.e.* is this novel paradigm worth pursuing).

5.1. COCO images

To determine (1), we needed a dataset with images containing multiple object category classes in order to assign all positive classes the same label, thus forming groundtruth saliency labels for each dataset. For evaluation purposes, we used the COCO 2017 dataset [38], which is a very popular benchmark for object detection, segmentation, and captioning. It is suitable for this study as it contains 164K large-size natural images and corresponding groundtruth labels with instance-level segmentation annotations from 80 common object classes. To investigate (2), we needed to compare the

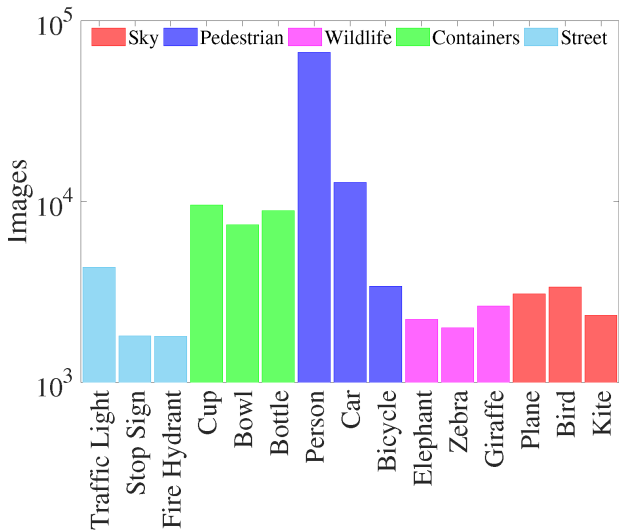


Figure 6: COCO subset distributions. This plot summarizes the 5 COCO 2017 subsets each containing three object class categories.

SC-RPN’s accuracy on different image resolutions across contextually different datasets.

5.2. Retinocollicular compression and re-labelling

En masse, (1) and (2) can be combined into a single experiment. Hence, we extracted 5 semantically different subsets from the COCO 2017 dataset based on the following selection criteria: (a) each subset must contain at least three contextually related and balanced (relatively uniform class instance distribution) object classes so that images have similar global properties, and (b) each subset must be quite different from the other subsets so that we can demonstrate how retinocollicular compression resolution varies depending on the dataset. Statistics of the resulting 5 datasets extracted from COCO 2017 are summarized in Figure 6.

Furthermore, 6 different resolutions, ranging between 16^2 and 512^2 pixels, of each subset were generated, totalling 30 new datasets. Resolutions below 16 or above 512 pixels were deemed unnecessary for our investigation. Concretely, we had training datasets D_i with $i \in \{1, 2, 3, 4, 5\}$ of square images of resolution $r \in \{16, 32, 64, 128, 256, 512\}^2$, I^r (see Figure 5-A), with associated labels L_I^r representing the instances of k objects present in I , with $k \subseteq C$, where C is the set of all positive object classes. In particular, L_I^r maps every image into a grayscale image of the same resolution r where the k -object instances are highlighted against the background by assigning each class a unique grayscale value (Figure 5-B). The downsampling method described in Section 4.1 were used

to transform original images from COCO resolution to each of these resolutions. We hypothesize that for a given dataset D , the optimal compression resolution $r_{optimal}$ exists in the range $\{16, 32, 64, 128, 256, 512\}^2$. We define $r_{optimal}$ here as the smallest resolution required to train a model without compromising its accuracy relative to training the same model on the highest resolution in the hyperparameter range yielding the highest accuracy.

Re-labelling of groundtruth images was subsequently performed in order to binarize the object class: $\forall L_I^r \mapsto BL_I^r, BL_I^r \in \mathbb{Z}_2^2$. BL_I^r maps every label L_I^r into a binary image of the same resolution (Figure 5-C). Finally, we follow common machine learning practice and divide each dataset into 70%, 20% and 10% for training, test and validation, respectively.

5.3. Training

For each of the aforementioned 30 datasets we trained a separate network instance using the SC-RPN architecture described in Section 4.2 on the training and validation images against the corresponding binarized saliency groundtruth labels BL_I^r . The SC-RPN’s FCN architecture used in this study is capable of generating saliency maps that are the same resolution as the input image, which was ideal for our experiment since we needed to train and compare the same network architecture on images of different resolutions without needing to change network or training hyperparameters, which always remained constant. The Python Keras API with the TensorFlow framework backend was used to implement and train each model on the respective subset training images end-to-end and from scratch (*i.e.* randomized initial weights). Network weights and parameters were initialized by seeding a pseudo-random number generator with the same seed for all training sessions and models to ensure repeatability and reproducibility⁴. The training images were propagated through the neural network in batches of 64. Weights were learned using stochastic gradient descent (RMSProp) over 100 epochs. The base learning rate was set to 0.05 and decreased by a factor of 10 every 2000 iterations. A mean-squared error loss function was implemented to compute loss for gradient descent. An NVIDIA Tesla K80 GPU was used for training and inference.

5.4. Evaluation metrics

Trained SC-RPNs were tested on their respective held-out test sets. The predicted labels from the models output were upsampled to match the dimensions of the ground truth labels of the highest resolution in the set (512×512 pixels) for a fair accuracy evaluation and comparison. Model accuracy was defined as a function of intersection over union (IoU) (Equation 1), where A_G is the pixel area

⁴Code included in the supplementary materials

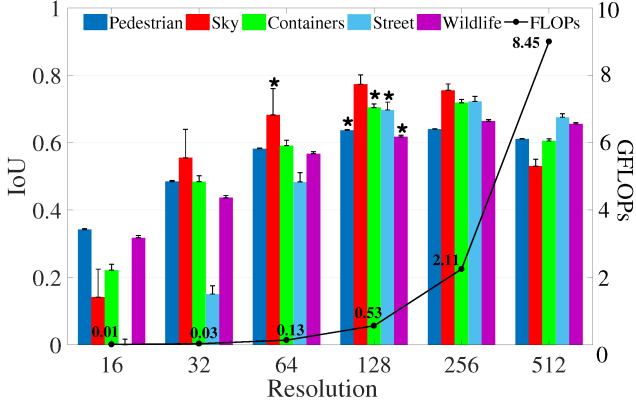


Figure 7: Dataset-specific resolution vs. IoU and FLOPs results. This histogram shows IoU results for each of the SC-FCN models trained separately on each of the 5 dataset at 6 different image resolutions and tested on the held-out test subsets of each dataset and resolution. Floating point operations (FLOPs) are also plotted for comparing number of computations between the resolutions. Asterisks indicate $r_{optimal}$ for a given dataset, defined as the minimum resolution yielding an IoU not statistically significantly different from the maximum IoU across all resolutions within each dataset. Bars represent means and error bars represent standard error of the mean.

of the ground truth bounding region, and A_P is the area of the predicted region. We did not adopt other common evaluation metrics, such as mean average precision (mAP), since saliency map proposals may include overlapping objects, and hence, regions containing multiple objects. We then performed two-tailed Students t -tests (with a null hypothesis of $p \leq 5\%$) between the highest accuracy resolution and the rest within each of the 5 subsets in order to identify $r_{optimal}$, which was then compared across all 5 subsets to determine if it varied depending on the dataset.

$$IoU = \frac{A_G \cap A_P}{A_G \cup A_P} \quad (1)$$

Finally, to determine (3) and (4), we needed to measure the SC-RPN’s computational costs and inference times across all 6 input resolutions. Consequently, detection time, defined as the average time taken by the model to generate a predicted saliency map based on each of the test images, and floating-point operations (FLOPs), defined in [39], were measured. FLOPs gives us a platform-independent measure of computation, which may not necessarily be linear with inference time for a number of reasons, such as caching, I/O, and hardware optimization [40].

6. Results

Figure 7 shows the dramatic reduction in computation cost from 10^9 FLOPs at 512×512 , which is representative of high-resolution input images used in most state-of-the-art detectors, to 10^7 FLOPs at 128×128 and 64×64 . Moreover, this significant computational cost saving comes at no significant accuracy cost, suggesting that identifying $r_{optimal}$ for a given dataset is an extremely valuable endeavour. Figure 8 complementarily echos the significant reduction in computational overheads by showing that the SC-RPN is capable of generating the complete set of region proposals at 500 frames/s. These figures are subsequently summarized and compared with state-of-the-art RPNs in Table 1.

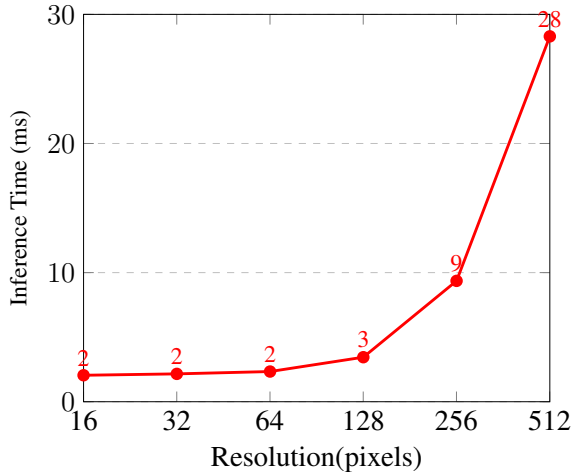


Figure 8: Inference time vs. resolution independent of dataset. This plot shows mean inference times for SC-RPNs trained and tested on each of the 5 dataset at 6 different image resolutions.

Figure 7 qualitatively shows four sets of example SC-RPN outputs (region proposal maps) from each group at 6 resolutions arranged from 512×512 to 16×16 . Predictions highlighted in red correspond to $r_{optimal}$ shown as asterisks in Figure 7. We observe that the SC-RPN is able to treat objects of different classes as the same saliency class (fourth row in each subset). We further observe that $r_{optimal}$ varies depending on the dataset (red saliency maps). It is also worth noting that among the five groups, three⁵ have predictions at 512×512 that are significantly worse than the best in each group. This suggests that high resolution images are not necessarily more accurate. A likely explanation might be that too much class-specific information is counter productive when the network is trying to learn to generalize features across different classes.

⁵Sky, Containers and Street

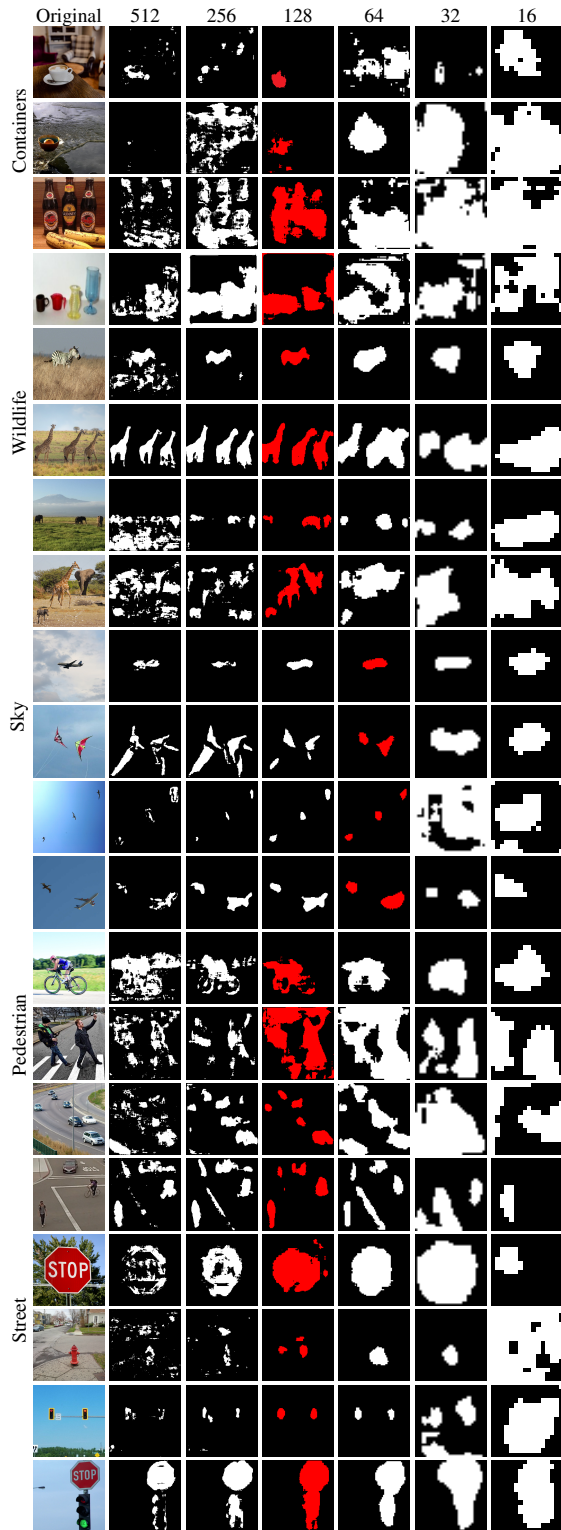


Figure 9: Qualitative results showing region proposals from SC-RPNs trained on different datasets and resolutions (columns). Each dataset has 4 sample images demonstrating the ability of models to predict saliency for images containing single and multiple classes. Red region proposals indicate $r_{optimal}$ for that particular dataset.

En masse, the reasonably high IoU scores and unprecedentedly low FLOPs observed in Figure 7, the enormous speed gains in Figure 8, the qualitative results in Figure 9, and last but not least, the unparalleled comparison with state-of-the-art RPNs in Table 1 suggests that the SC-RPN can accurately propose object-only regions using significantly fewer computational resources at significantly faster speeds compared to state-of-the-art RPNs. Therefore, these results support the hypotheses that: (1) the SC-RPN is able to correctly assign saliency to all the original object-only classes; and (2) the optimal input resolution $r_{optimal}$ is dataset dependent and (3) requires significantly fewer computations.

7. Conclusions

This paper exposed a common bottleneck in state-of-the-art object detection models, which has thus far impeded their practical adoption, especially on embedded systems. After thoroughly and carefully researching the visual neuroscience literature, particularly on the superior colliculus, selective attention, and the retinocollicular visual pathway, we discovered new, overlooked knowledge that gave us new insights into the mechanisms underlying speed and efficiency in detecting objects in biological vision systems. Specifically, we learned that a midbrain structure known as the superior colliculus receives heavily-reduced achromatic visual information from the eye, which it then uses to compute a saliency map that highlights object-only regions for further cognitive analyses. We also learned that the degree of visual information reduction is species-dependent and consequently dependent on the visual environment; thereby, allowing us to think of object detection training datasets in a similar manner.

We then leveraged these insights to design and imple-

Model	Size (MB)	GFLOPs	Frames/s
SSD	104	91	20
RetinaNet	332	78	8
TinySSD	2.3	1.2	23
YOLO	753	213	9
Tiny YOLO	61	7	17
Faster R-CNN	523	172	9
MobileNet	22	1	30
SC-RPN	0.57	0.13	500

Table 1: Comparing SC-RPN’s size, efficiency and speed with state-of-the-art models [40]. The comparison is based on three key aspects: (1) memory required to store network parameters measured in Megabytes; (2) computational cost measured in Giga FLOPs; and (3) inference speed measured in frames per second using an NVIDIA Tesla K80 GPU.

ment a region proposal model based on selective attention that demonstrably significantly reduces computational costs in object detection without compromising detection accuracy. Furthermore, our results suggest that this bio-inspired model outperforms the computational costs of state-of-the-art region proposal networks by two to three orders of magnitude in terms of inference speed and FLOPs. Therefore, we conclude by proposing our model and methodology for designing practical and efficient deep learning object detection networks for embedded devices.

A promising future direction to explore is an optimization algorithm that automatically learns the optimal input resolution (*i.e.* degree of visual compression) required by the superior colliculus RPN to only detect classes-of-interest from a given dataset, while ignoring background regions; thus optimizing the overall region proposal pipeline in an end-to-end fashion.

8. Acknowledgements

This research was supported by an Australian Postgraduate Award scholarship and the Professor Robert and Josephine Shanks scholarship.

References

- [1] N. Tijtgat, W. V. Ranst, B. Volckaert, T. Goedem, and F. D. Turck, "Embedded Real-Time Object Detection for a UAV Warning System," in *IEEE International Conference on Computer Vision Workshops (ICCVW)*, pp. 2110–2118, Oct. 2017.
- [2] S. Ren, K. He, R. Girshick, and J. Sun, "Faster R-CNN: Towards Real-Time Object Detection with Region Proposal Networks," in *Advances in Neural Information Processing Systems (NIPS) 28* (C. Cortes, N. D. Lawrence, D. D. Lee, M. Sugiyama, and R. Garnett, eds.), pp. 91–99, Curran Associates, Inc., 2015.
- [3] J. Redmon, S. Divvala, R. Girshick, and A. Farhadi, "You Only Look Once: Unified, Real-Time Object Detection," in *IEEE Conference on Computer Vision and Pattern Recognition (CVPR)*, pp. 779–788, June 2016.
- [4] W. Liu, D. Anguelov, D. Erhan, C. Szegedy, S. Reed, C.-Y. Fu, and A. C. Berg, "SSD: Single Shot MultiBox Detector," in *Proceedings of the European Conference on Computer Vision (ECCV)* (B. Leibe, J. Matas, N. Sebe, and M. Welling, eds.), Lecture Notes in Computer Science, pp. 21–37, Springer International Publishing, 2016.
- [5] M. Gao, R. Yu, A. Li, V. I. Morariu, and L. S. Davis, "Dynamic Zoom-In Network for Fast Object Detection in Large Images," in *Proceedings of the IEEE Conference on Computer Vision and Pattern Recognition (CVPR)*, pp. 6926–6935, 2018.
- [6] P. Tang, X. Wang, A. Wang, Y. Yan, W. Liu, J. Huang, and A. Yuille, "Weakly Supervised Region Proposal Network and Object Detection," in *Proceedings of the European Conference on Computer Vision (ECCV)*, pp. 352–368, 2018.
- [7] T.-Y. Lin, P. Goyal, R. Girshick, K. He, and P. Dollar, "Focal Loss for Dense Object Detection," in *Proceedings of the IEEE International Conference on Computer Vision (ICCV)*, pp. 2980–2988, 2017.
- [8] A. Shrivastava, A. Gupta, and R. Girshick, "Training Region-Based Object Detectors With Online Hard Example Mining," in *Proceedings of the IEEE Conference on Computer Vision and Pattern Recognition*, pp. 761–769, 2016.
- [9] A. Wong, M. J. Shafiee, F. Li, and B. Chwyl, "Tiny SSD: A Tiny Single-shot Detection Deep Convolutional Neural Network for Real-time Embedded Object Detection," Feb. 2018.
- [10] B. Wu, F. Iandola, P. H. Jin, and K. Keutzer, "SqueezeDet: Unified, Small, Low Power Fully Convolutional Neural Networks for Real-Time Object Detection for Autonomous Driving," in *IEEE Conference on Computer Vision and Pattern Recognition Workshops (CVPRW)*, pp. 446–454, July 2017.
- [11] S. Yohanandan, A. Song, A. G. Dyer, and D. Tao, "Saliency Preservation in Low-Resolution Grayscale Images," in *Proceedings of the European Conference on Computer Vision (ECCV)* (V. Ferrari, M. Hebert, C. Sminchisescu, and Y. Weiss, eds.), Lecture Notes in Computer Science, pp. 237–254, Springer International Publishing, 2018.
- [12] L. Itti, C. Koch, and E. Niebur, "A model of saliency-based visual attention for rapid scene analysis," in *IEEE Transactions on Pattern Analysis and Machine Intelligence (PAMI)*, vol. 20, pp. 1254–1259, Nov. 1998.
- [13] J. Zhu, J. Wu, Y. Xu, E. Chang, and Z. Tu, "Unsupervised Object Class Discovery via Saliency-Guided Multiple Class Learning," in *IEEE Transactions on Pattern Analysis and Machine Intelligence (PAMI)*, vol. 37, pp. 862–875, Apr. 2015.
- [14] C. Wang and B. Yang, "Saliency-guided object proposal for refined salient region detection," in *Visual Communications and Image Processing (VCIP)*, pp. 1–4, Nov. 2016.
- [15] L. Duan, J. Gu, Z. Yang, J. Miao, W. Ma, and C. Wu, "Bio-inspired Visual Attention Model and Saliency Guided Object Segmentation," in *Genetic and Evolutionary Computing* (J.-S. Pan, P. Krmer, and V. Snel, eds.), Advances in Intelligent Systems and Computing, pp. 291–298, Springer International Publishing, 2014.
- [16] A. Fattal, M. Karg, C. Scharfenberger, and J. Adamy, "Saliency-guided region proposal network for CNN based object detection," in *IEEE 20th International Conference on Intelligent Transportation Systems (ITSC)*, pp. 1–8, Oct. 2017.
- [17] M. Guo, Y. Zhao, C. Zhang, and Z. Chen, "Fast object detection based on selective visual attention," in *Neurocomputing*, vol. 144, pp. 184–197, Nov. 2014.
- [18] V. H. Perry and A. Cowey, "Retinal ganglion cells that project to the superior colliculus and pretectum in the macaque monkey," in *Neuroscience*, vol. 12, pp. 1125–1137, Aug. 1984.

- [19] R. Veale, Z. M. Hafed, and M. Yoshida, "How is visual saliency computed in the brain? Insights from behaviour, neurobiology and modelling," in *Phil. Trans. R. Soc. B*, vol. 372, p. 20160113, Feb. 2017.
- [20] B. J. White, D. J. Berg, J. Y. Kan, R. A. Marino, L. Itti, and D. P. Munoz, "Superior colliculus neurons encode a visual saliency map during free viewing of natural dynamic video," in *Nature Communications*, vol. 8, p. 14263, Jan. 2017.
- [21] B. J. White, J. Y. Kan, R. Levy, L. Itti, and D. P. Munoz, "Superior colliculus encodes visual saliency before the primary visual cortex," in *Proceedings of the National Academy of Sciences*, p. 201701003, Aug. 2017.
- [22] L. Siklssy and E. Tulp, "The space reduction method: a method to reduce the size of search spaces," in *Information Processing Letters*, vol. 38, pp. 187–192, May 1991.
- [23] A. Krizhevsky, I. Sutskever, and G. E. Hinton, "ImageNet Classification with Deep Convolutional Neural Networks," in *Advances in Neural Information Processing Systems 25* (F. Pereira, C. J. C. Burges, L. Bottou, and K. Q. Weinberger, eds.), pp. 1097–1105, Curran Associates, Inc., 2012.
- [24] J. R. R. Uijlings, K. E. A. van de Sande, T. Gevers, and A. W. M. Smeulders, "Selective Search for Object Recognition," in *International Journal of Computer Vision (IJCV)*, vol. 104, pp. 154–171, Sept. 2013.
- [25] J. Hosang, R. Benenson, P. Dollr, and B. Schiele, "What Makes for Effective Detection Proposals?," in *IEEE Transactions on Pattern Analysis and Machine Intelligence (PAMI)*, vol. 38, pp. 814–830, Apr. 2016.
- [26] K. He, G. Gkioxari, P. Dollr, and R. Girshick, "Mask R-CNN," in *2017 IEEE International Conference on Computer Vision (ICCV)*, pp. 2980–2988, Oct. 2017.
- [27] K. He, X. Zhang, S. Ren, and J. Sun, "Deep Residual Learning for Image Recognition," pp. 770–778, 2016.
- [28] T. Lin, P. Dollr, R. Girshick, K. He, B. Hariharan, and S. Belongie, "Feature Pyramid Networks for Object Detection," in *2017 IEEE Conference on Computer Vision and Pattern Recognition (CVPR)*, pp. 936–944, July 2017.
- [29] A. Shrivastava, R. Sukthankar, J. Malik, and A. Gupta, "Beyond Skip Connections: Top-Down Modulation for Object Detection," in *arXiv:1612.06851 [cs]*, Dec. 2016. arXiv: 1612.06851.
- [30] J. Redmon and A. Farhadi, "YOLO9000: Better, Faster, Stronger," in *arXiv:1612.08242 [cs]*, Dec. 2016. arXiv: 1612.08242.
- [31] H. Karaoguz and P. Jensfelt, "Fusing Saliency Maps with Region Proposals for Unsupervised Object Localization," in *arXiv:1804.03905 [cs]*, Apr. 2018. arXiv: 1804.03905.
- [32] T. Moore and M. Zirnsak, "Neural Mechanisms of Selective Visual Attention," in *Annual Review of Psychology*, vol. 68, pp. 47–72, Jan. 2017.
- [33] H. Okawa and A. P. Sampath, "Optimization of single-photon response transmission at the rod-to-rod bipolar synapse," in *Physiology*, vol. 22, pp. 279–286, Aug. 2007.
- [34] L. D. Silverstein, "Foundations of Vision, by Brian A. Wandell, Sinauer Associates, Inc., Sunderland, MA, 1995. xvi + 476 pp., hardcover \$49.95.," in *Color Research & Application*, vol. 21, pp. 142–144, Apr. 1996.
- [35] V. H. Perry, R. Oehler, and A. Cowey, "Retinal ganglion cells that project to the dorsal lateral geniculate nucleus in the macaque monkey," in *Neuroscience*, vol. 12, pp. 1101–1123, Aug. 1984.
- [36] T. Judd, F. Durand, and A. Torralba, "Fixations on low-resolution images," in *Journal of Vision*, vol. 11, pp. 1–20, Apr. 2011.
- [37] J. Long, E. Shelhamer, and T. Darrell, "Fully convolutional networks for semantic segmentation," in *IEEE Conference on Computer Vision and Pattern Recognition (CVPR)*, pp. 3431–3440, June 2015.
- [38] T.-Y. Lin, M. Maire, S. Belongie, J. Hays, P. Perona, D. Ramanan, P. Dollr, and C. L. Zitnick, "Microsoft COCO: Common Objects in Context," in *Proceedings of the European Conference on Computer Vision (ECCV)* (D. Fleet, T. Pajdla, B. Schiele, and T. Tuytelaars, eds.), Lecture Notes in Computer Science, pp. 740–755, Springer International Publishing, 2014.
- [39] M. Thoma, "Analysis and Optimization of Convolutional Neural Network Architectures," in *arXiv:1707.09725 [cs]*, July 2017. arXiv: 1707.09725.
- [40] J. Huang, V. Rathod, C. Sun, M. Zhu, A. Korattikara, A. Fathi, I. Fischer, Z. Wojna, Y. Song, S. Guadarrama, and K. Murphy, "Speed/Accuracy Trade-Offs for Modern Convolutional Object Detectors," in *2017 IEEE Conference on Computer Vision and Pattern Recognition (CVPR)*, pp. 3296–3297, July 2017.